CHAPTER II

Ray Equations In Retarded Snell Midpoint Coordinates

2.1. Introduction.

Group velocity equations represent asymptotic descriptions of wave operators in the high frequency limit. They may be used to study the motion of energy when wavefields are extrapolated in depth. In this chapter we derive a method of finding group velocity equations from any given wave equation.

Specifically we apply the method to find group velocity equations for wave equation operators in retarded Snell midpoint coordinates. This coordinate system is convenient for the velocity estimation problem. Since all wavefield extrapolation operators require a background velocity to be specified, we use ray equations to analyze their sensitivity to velocity.

We start the chapter finding group velocity equations for the exact two–dimensional acoustic wave equation and two of its one–way approximations. Next we use the definition of retarded Snell midpoint coordinates to transform these group velocity equations to the new coordinate system. The velocity dependence of wave equations is discussed along with their group velocity equations.

2.2. Group velocity equations from wave equations.

Given a gather in half offset–time (h,t) space, in the process of downward continuation to zero time and zero offset, energy must move along the group velocity lines. For constant velocity these lines will be straight. They can be determined by application of the formal ray–tracing equation (Cerveny *et al*

1977, Yedlin 1978). Such equations are valid when there is anisotropy and the direction of the phase velocity vector is not the same as the group velocity vector. Another advantage of direct application of the ray–tracing equations is that they can be transformed into any coordinate system. In what follows, the ray equation will be derived and then applied to the problem of imaging. For ray tracing the amplitudes are not calculated, but these can be qualitatively determined by looking at the instantaneous ray density.

The general ray tracing equations, which will be derived for a two–dimensional constant velocity medium, can be best obtained by using the dispersion relation for the particular wave equation under consideration. Let us consider a general dispersion relation of the form:

$$F(p,q) = 0 \tag{2.1}$$

where ω is the frequency,

$$p = k_h / \omega \tag{2.2a}$$

$$q = k_z / \omega \tag{2.2b}$$

and k_h = horizontal wavenumber, k_z = vertical wavenumber.

The frequency is scaled out of the dispersion relation, as we do not want our ray trace equations to have any explicit frequency dependence. Also it is convenient to work in slowness coordinates, which are the duals of the displacement coordinates.

Now consider a ray whose coordinates (h,z), are parameterized by the time t along the ray. Then the components of the tangent vector to the ray are proportional to the group velocity. The group velocity, in turn, is proportional to the normal derivatives of the dispersion relation, $F(p,q) = 0$. Therefore, (figure 2.1)

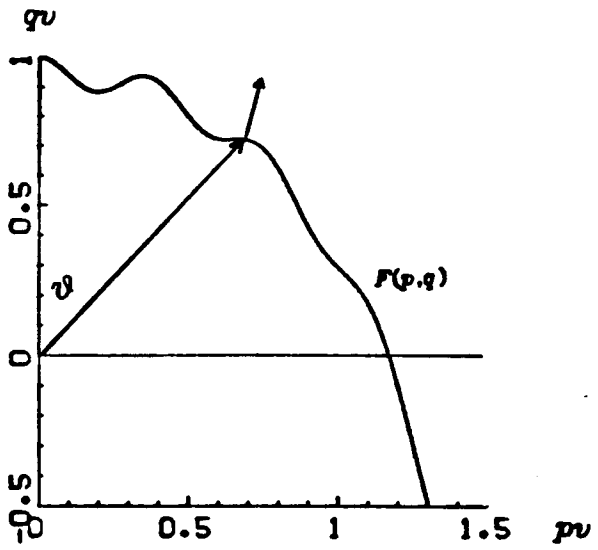

FIGURE 2.1. Phase and group velocities. $F(p,q)$ represents the dispersion relation for a given wave equation. The direction of the *phase velocity* for a fixed angle ϑ is given by the position vector to the dispersion relation F, while the direction of the *group velocity* is given by the *normal* vector at F.

$$\frac{dh}{dt} = \lambda \frac{\partial F}{\partial p} \tag{2.3a}$$

$$\frac{dz}{dt} = \lambda \frac{\partial F}{\partial q} \tag{2.3b}$$

For most situations, it is easy to calculate $\frac{\partial F}{\partial p}$ and $\frac{\partial F}{\partial q}$.

The parameter λ can be evaluated by looking at the definition of a wavefront. A wavefront is defined to be the locus of points such that at a particular time, $t = \tau(h,z)$ defines the location of the wavefront. Differentiating this function τ with respect to t using the chain rule, we get

$$1 = \frac{\partial \tau}{\partial h}\frac{dh}{dt} + \frac{\partial \tau}{\partial z}\frac{dz}{dt} \tag{2.4}$$

The quantities $\frac{\partial \tau}{\partial h}$ and $\frac{\partial \tau}{\partial z}$ are the wavefront normal components p and q. Substitution of equation (2.3) into equation (2.4) results in:

$$\lambda = \frac{1}{p\frac{\partial F}{\partial p} + q\frac{\partial F}{\partial q}} \tag{2.5}$$

The formalism of equations (2.3), (2.4) and (2.5) is convenient in that it can be applied to any dispersion relation. There is no need to get involved in complicated geometric projections, as happens if the dispersion relation departs from a circle.

TABLE (3.1) Ray equations. Non–slanted wave propagation.

	$F(p,q)$	dh/dt	dz/dt
90^0	$p^2 + q^2 - \frac{1}{v^2}$	pv^2	qv^2
15^0	$q + \frac{p^2 v}{2} - \frac{1}{v}$	$\frac{2pv^2}{p^2v^2+2}$	$\frac{2v}{p^2v^2+2}$
45^0	$q - \frac{1}{v}\frac{1-\frac{3}{4}p^2v^2}{1-\frac{1}{4}p^2v^2}$	$\frac{pv^2}{1+\frac{3}{16}p^4v^4}$	$\frac{v(1-\frac{1}{4}p^2v^2)^2}{1+\frac{3}{16}p^4v^4}$

2.3. Examples in non-retarded, non-slanted coordinates.

Table (3.1) summarizes the ray equations derived in Appendix (A) for the non–retarded, non–slanted acoustic wave equation and its one–way fifteen and forty–five degree approximations.

In figure (3.1) the dispersion relations are plotted. The exact case is a semicircle. Figure (3.2) plots the group velocity equations. The exact case gives straight lines when the velocity is constant.

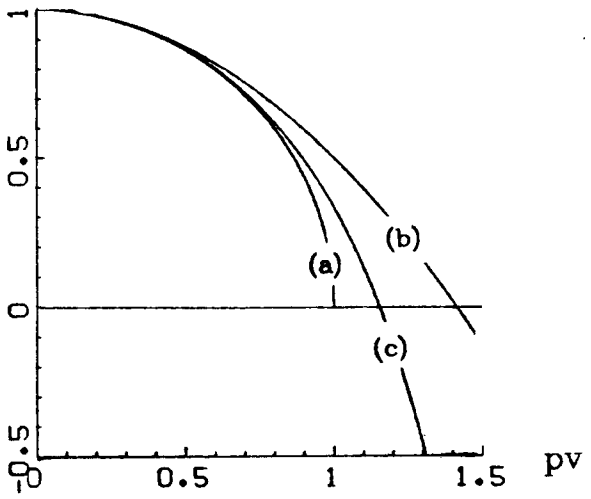

FIGURE 3.1. Dispersion relations. Positive quadrant for the dispersion relations of the (a) exact, (b) fifteen, and (c) forty–five wave equations.

A convenient way to see how these equations move energy when downward continuing events in *CMP* gathers is the following: start with some event representing the arrival times from a given reflector. In the high frequency limit where ray equations are valid, to every arbitrarily small neighborhood about a fixed arrival point of an event, there is an associated value of the ray parameter p. In constant velocity most of the energy converging at that point has been propagated with a fixed angle. We can fix this angle and follow the trajectory of the energy as downward continuation proceeds. For the figures we will draw trajectories for several angles of propagation at every other Δz step.

For the exact acoustic wave equation, figure (3.3) shows group velocity trajectories as a function of angle for a given event at different velocities of extrapolation. In the first case, (figure 3.3a), when the event and operator velocities match, the energy at all angles moves toward the origin. There is a depth where all the energy is at the origin. At this depth we define the image of the event. Once the depth of imaging has been passed, the energy diffracts back to

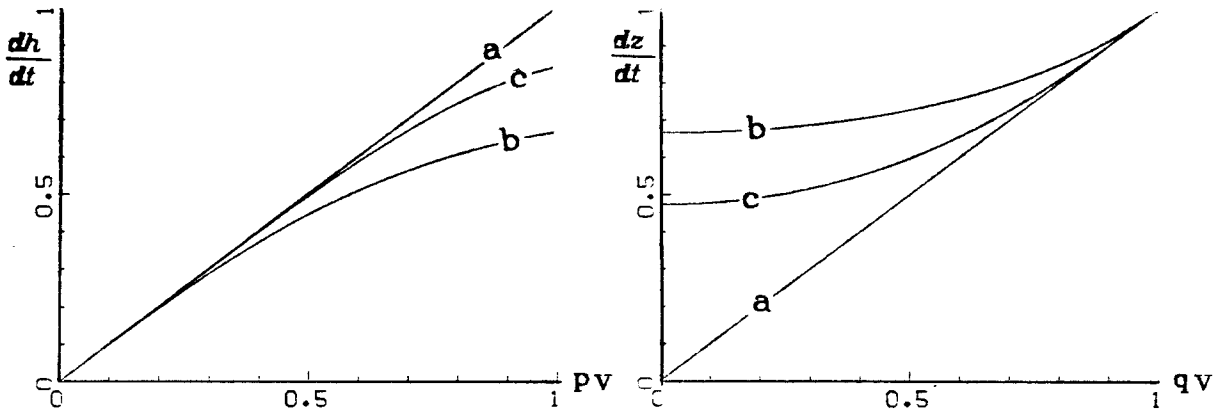

FIGURE 3.2. Group velocity equations. (a) exact, (b) fifteen, and (c) forty–five wave equations.

negative times.

In the second case, (figure 3.3b), the operator velocity has been underestimated by 5%. The imaging principle is applied when $t = 0$ is reached extrapolating with the operator velocity. Because of the velocity error, the energy is still unfocused when we reach the time origin. The energy in the imaged gather will appear smeared over several offsets. The best focus occurs at the time when the depth of the event is reached, not when we apply the imaging principle. Even at this time the velocity error prevents all rays to converge in phase to zero offset. An exact operator can only give a perfect focus when the exact velocity is used, otherwise it can only approximately image the energy.

The third case, (figure 3.3c) is similar to the second, with velocity overestimated by 5%. The energy is best focused at the true depth, not when we apply the imaging principle at $t = 0$ according to the operator velocity. Again, the best focus is not only at the wrong time, but appears blurred as well.

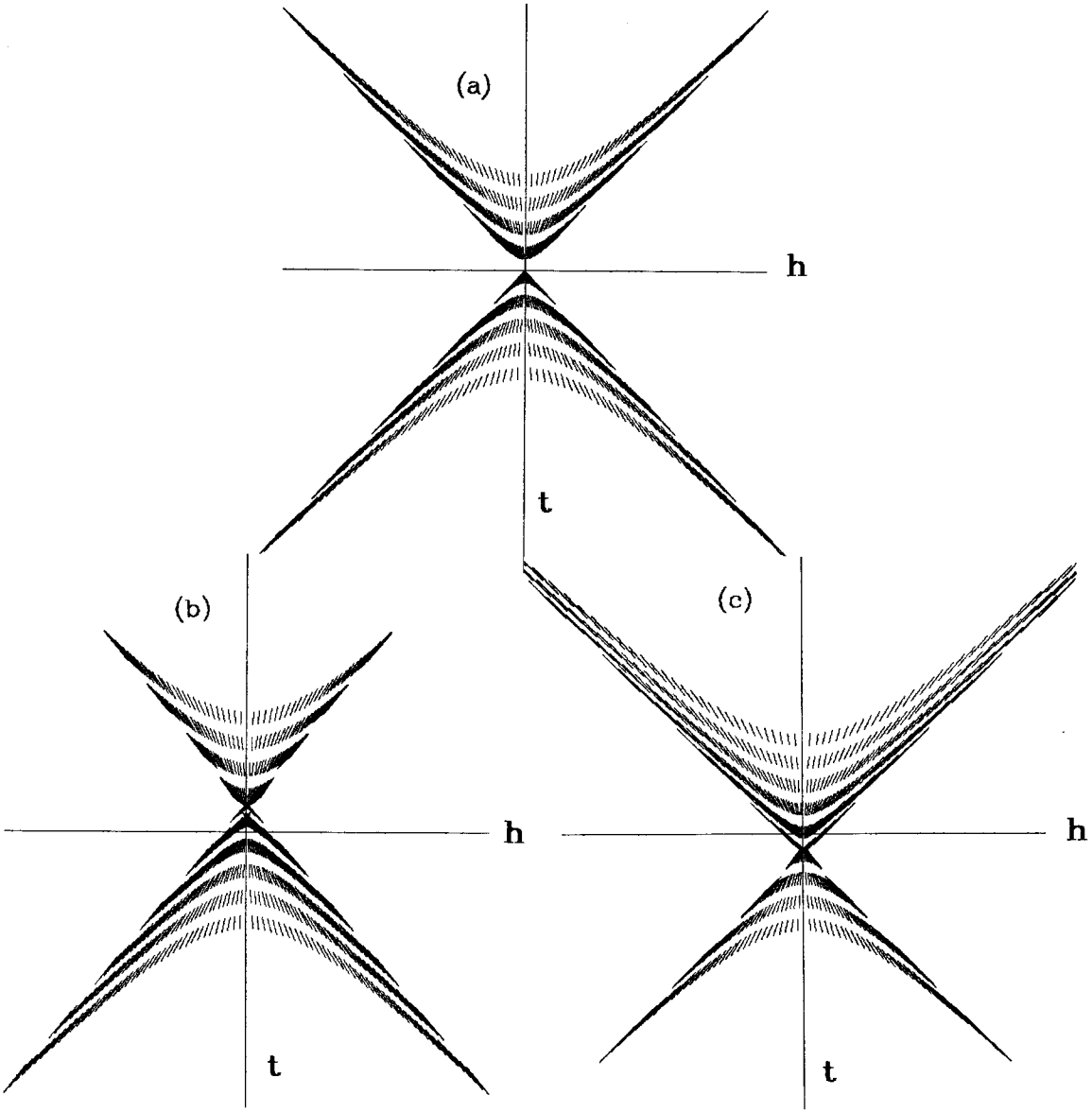

FIGURE 3.3. Imaging, ninety degree. This figure illustrates the way energy moves in the (h,t) plane as we extrapolate with the 90 *degree* wave equation. The figure was computed starting with some hyperbolic event for a fixed depth, subsequently extrapolating the wavefront using the ray equations. The process was done at fixed increments of *depth*, represented as slashed lines in the figure. In (a) the extrapolation was done with the same velocity as used to generate the hyperbolic event. We get a perfect image at $t = 0$ since all the rays are traveling at the correct speed for all angles. In (b) we used a 5 % lower velocity in the extrapolation. Now the energy is imaging at $t < 0$. However, now the speed at which the wavefront moves has become p –dependent, and we no longer achieve a perfect image. In (c) the extrapolation velocity was 5% higher. Now the image is at $t > 0$ and again the wavefront velocity is dependent on p, a blurred image is obtained.

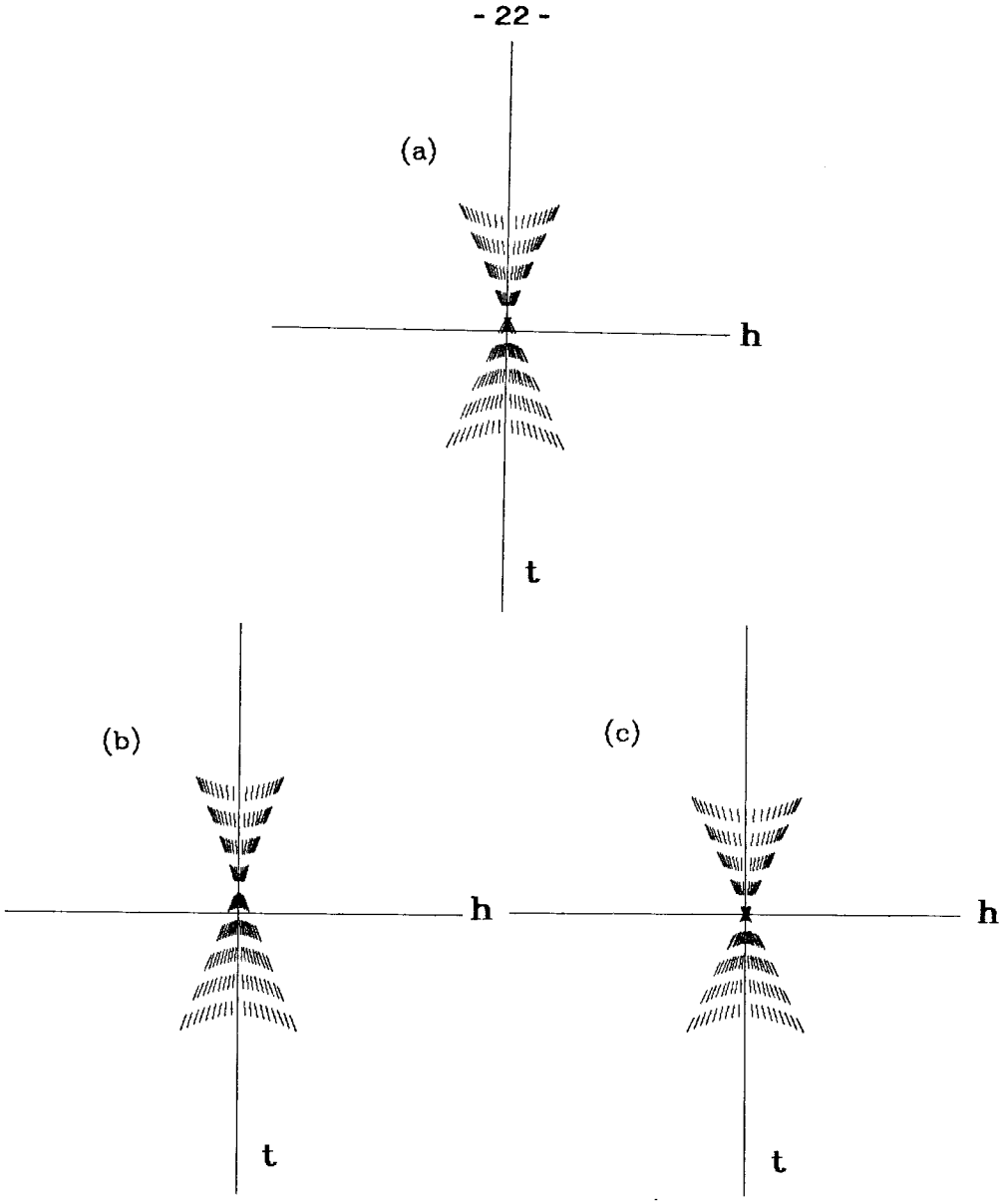

FIGURE 3.4. Imaging, fifteen degree. In this figure we are extrapolating the wavefront with the 15 degree equation. The figure was computed using angles $\vartheta < 30^0$. We are again extrapolating the wavefield at fixed increments of depth, represented by broken lines in the figure. In (a) the extrapolation velocity equals the event velocity. We can check that for angles close to 0^0 the energy arrives close to $t = 0$. For wider angles the energy is traveling slower than required for correct imaging. In (b) the extrapolation velocity is 5 % slower, so energy images at $t < 0$. In (c) the extrapolation velocity is 5 % faster. The rays close to 0^0 image earlier in time. Since the 15 degree equation moves energy slower than required for wider angles, the apparent best imaging occurs with this higher velocity than with the exact velocity. This is associated with the effect shown in figure (3.2), where the group velocity for the approximate operator is less or equal to the group velocity for the exact operator.

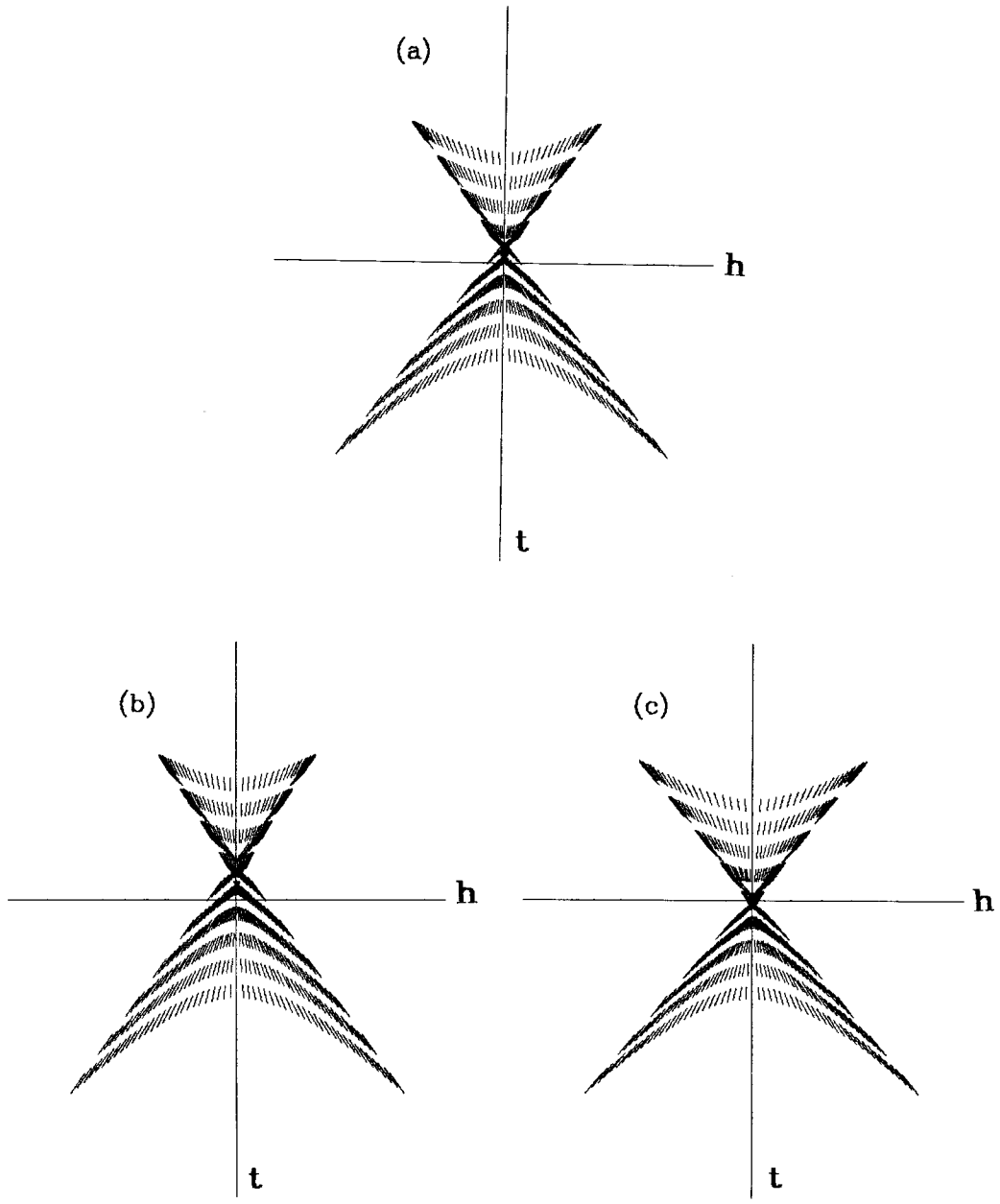

FIGURE 3.5. Imaging, forty–five degree. Extrapolation with the 45 *degree* equation. The figure was computed using angles $\vartheta < 60^0$. Note in particular that the position of the image has been improved when the velocity is correct, but we still need higher velocity to get better image. Velocities are the same as in figure (3.4).

For the fifteen degree equation the ray equations have 5% error when $\vartheta \approx 30^0$ (figure 3.2). The approximate operator moves the energy slower than the exact operator, this effect increasing with angle.

Figure (3.4) illustrates the behavior of the operator associated with the fifteen degree ray equations. We plot the situations when the operator velocity is exact and when there is 5% under and over estimation in velocity. The decrease in the group velocity of the operator with respect to the exact group velocity is seen. Better imaging is obtained when velocity is overestimated.

For the forty–five degree equation, (figure 3.5), the group velocity is still slower than the exact one, but now we get 5% error for $\vartheta \approx 60^0$.

Note in particular that when the extrapolation velocity is incorrect, the image obtained with the approximate one–way equations is nearly as good as the image given by the exact operator with the same incorrect velocity.

2.4. Group Velocity Equations in Retarded Snell Midpoint Coordinates.

Retarded Snell midpoint coordinates are a suitable frame of reference for studying slanted wave propagation. These coordinates are also a natural frame of reference for velocity estimation problems. Because of the importance of Snell coordinates, we derive group velocity equations for the wave equation in this coordinate frame. The ray equations will allow us to better understand how our wave operators move the energy when used to image *CMP* gathers.

Using the notation defined in figure (4.1). The coordinates are defined as follows: (one–way travel time)

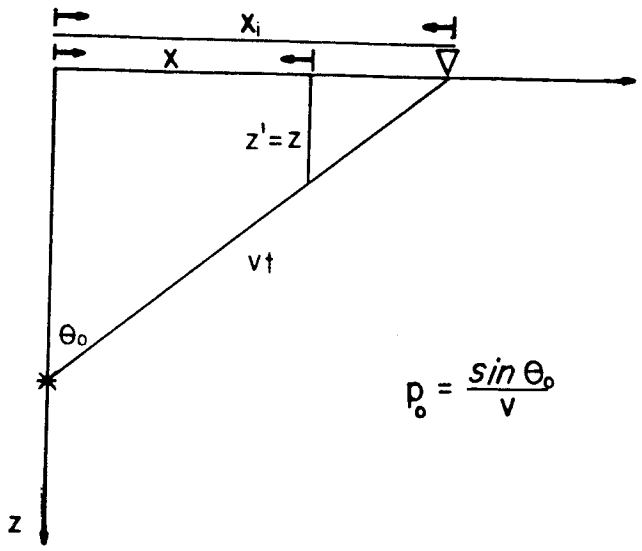

FIGURE 4.1. Slant wave propagation geometry.

$$t' = t - p_0 h + \frac{z\cos\vartheta_0}{v} \tag{4.1a}$$

$$h' = h + z\tan\vartheta_0 \tag{4.1b}$$

$$z' = z \tag{4.1c}$$

The utility the above coordinate derives is that, for the particular p_0 chosen, h' is fixed as we downward continue. Also, the imaging condition for t' is simply $t' = \frac{z\cos\vartheta_0}{v}$. Applying the transformation (4.1) to the original data and migrating keeps the top of the new skewed hyperbola fixed. This result is useful in velocity analysis.

Before proceeding, we need to fix the sign convention. From figure (4.1), we notice that both dt and dh are negative when we project the ray from the geophone back to the source. $\frac{dh}{dt}$ is positive. Similarly, as t is decreasing, z' is increasing. Therefore,

$$sgn\left[\frac{dh}{dt}\right] = -sgn\left[\frac{dz}{dt}\right] \tag{4.2}$$

To find the appropriate ray equations in the new coordinate system, we need to compute $\frac{dh'}{dt'}$ and $\frac{dz'}{dt'}$. Application of the chain rule to h' in equation (4.1) results in

$$\frac{dh'}{dt} = \frac{dh}{dt} + \frac{dz}{dt}\tan\vartheta_0 \tag{4.3a}$$

$$\frac{dz'}{dt} = \frac{dz}{dt} \tag{4.3b}$$

but

$$\frac{dh'}{dt} = \frac{dh'}{dt'}\frac{dt'}{dt} \tag{4.4a}$$

$$\frac{dz'}{dt} = \frac{dz'}{dt'}\frac{dt'}{dt} \tag{4.4b}$$

Substituting these results into equation (4.3), writing the tangent and cosine as function of p and q, $\tan\vartheta_0 = \frac{p_0}{q_0}$, $\cos\vartheta_0 = q_0 v$, and taking care of the sign convention, we get

$$\frac{dh'}{dt'} = \left[\left|\frac{dh}{dt}\right| - \left|\frac{dz}{dt}\right|\frac{p_0}{q_0}\right]\left[\frac{dt'}{dt}\right]^{-1} \tag{4.5a}$$

$$\frac{dz'}{dt'} = \left[\frac{dz}{dt}\right]\left[\frac{dt'}{dt}\right]^{-1} \tag{4.5b}$$

The $\frac{dt'}{dt}$ derivative is obtained using equation (4.1):

$$\frac{dt'}{dt} = 1 - p_0 \left| \frac{dh}{dt} \right| - q_0 \left| \frac{dz}{dt} \right| \tag{4.5c}$$

Finally we need to find transformation equations for p' and q' for the new coordinate frame. For this we use equation (4.1) and find that

$$\left.\frac{\partial t'}{\partial h'}\right|_z = \left.\frac{\partial t}{\partial h}\frac{\partial h}{\partial h'}\right|_z - p_0$$

For z fixed $\left.\frac{\partial h}{\partial h'}\right|_z = 1$. Therefore

$$\left.\frac{\partial t}{\partial h}\right|_z = \left.\frac{\partial t'}{\partial h'}\right|_z + p_0$$

Of course $\left.\frac{\partial t}{\partial h}\right|_z$ is p.

If all the variables are seen in the slanted coordinate system, we need to replace p and q with

$$p = p' + p_0 \tag{4.6a}$$

$$q = \frac{1}{v}\left[1 - v^2 (p' + p_0)^2\right]^{1/2} \tag{4.6b}$$

where p' is the measured $\left.\frac{\partial t'}{\partial h'}\right|_z$.

With p, q and the sign convention determined, equations (4.5) and (4.6) allow us to find ray equations in the new coordinate frame as a function of the ray equations in the standard reference frame that was used in section (2).

2.5. Examples in Retarded Snell Midpoint Coordinates.

Table (5.1) summarizes the group velocity equations transformed into Snell midpoint coordinates using the rules of transformation derived in section (4).

We start illustrating the behavior of energy in this new coordinate system with a non-slanted example. Figure (5.1) shows downward continuation with reference ray parameter $p_0 = 0$ using the exact acoustic wave equation. Here the only effect the coordinate transformation has is time retardation by

TABLE (5.1) Ray equations. Slanted wave propagation.

	dh'/dt'	dz'/dt'
90^0	$\dfrac{q_0 pv^2 - p_0 qv^2}{q_0[1 - p_0 pv^2 - q_0 qv^2]}$	$\dfrac{qv^2}{[1 - p_0 pv^2 - q_0 qv^2]}$
15^0	$\dfrac{v(pv - p_0/q_0)}{1 + \frac{1}{2}p^2v^2 - pp_0v^2 - q_0v}$	$\dfrac{v}{1 + \frac{1}{2}p^2v^2 - pp_0v^2 - q_0v}$
45^0	$\dfrac{pv^2 - \frac{p_0}{q_0}v(1 - \frac{1}{4}p^2v^2)^2}{\text{den45}}$	$\dfrac{v(1 - \frac{1}{4}p^2v^2)^2}{\text{den45}}$
$p = p' + p_0$		
$q = \dfrac{1}{v}[1 - v^2(p' + p_0)^2]^{1/2}$		
$\text{den45} = 1 + \dfrac{3}{16}p^4v^4 - p_0pv^2 - q_0v\,(1 - \dfrac{1}{4}p^2v^2)^2$		

$z \cos\vartheta_0 / v$. The image is still defined at $t = 0$, translating to $t' = \tau = z \cos\vartheta_0 / v$ in the retarded frame. The zero offset arrival does not move as downward continuation proceeds.

In figure (5.2) the slanted case is illustrated with the exact downward continuation operator. First notice that the $p' = 0$ point of the event remains fixed as the extrapolation proceeds. This $p' = 0$ point remains stationary, independently of whether the extrapolation velocity was incorrect. When the velocity is exact we get a prefect image; all the energy converges to the same point at the same depth. When there are errors in velocity we can only expect a blurred image.

Figure (5.2) shows how the linear moveout correction has increased the stepout (higher p') in the negative range of offsets while it has decreased the stepout for the positive range of offsets. Group velocity equations and their associated operators are more sensitive to errors in velocity for higher stepouts. In a typical field data gather only positive offsets are available. These offsets are where there has been a decrease in relative stepout. We expect operators in Snell coordinates to be less sensitive to velocity than non–slanted operators. This is an advantage when imaging gathers for velocity estimation.

Figure (5.3) illustrates the use of the fifteen degree group velocity equations. Imaging has now become less dependent on velocity, even though we are plotting angles of propagation up to 60^0 (about p_0).

Figure (5.4) illustrates the forty–five degree approximation behavior for the group velocity equations. Now we have more sensitivity to the operator velocity. The size of the zone where the image occurs is wider.

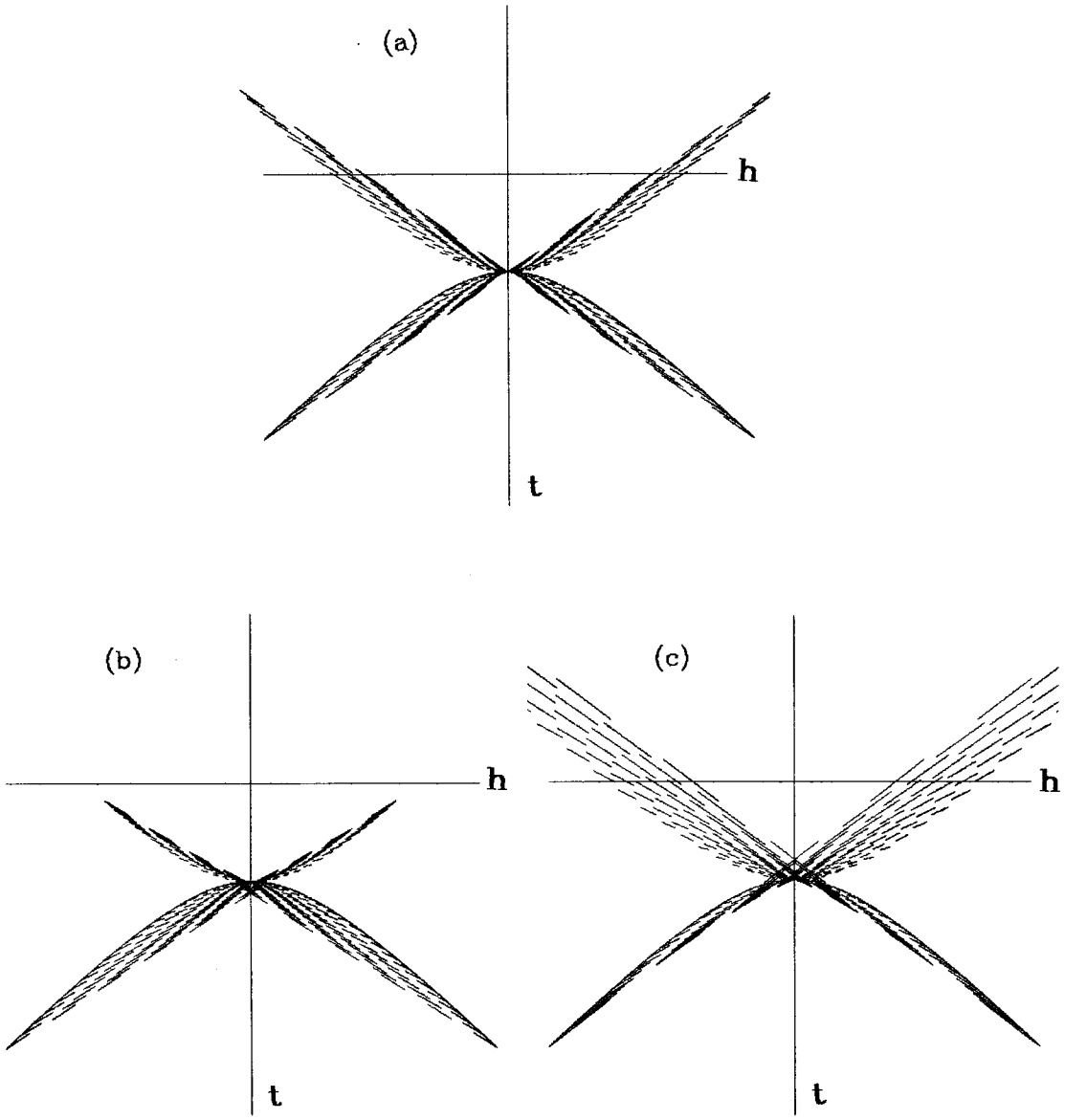

FIGURE 5.1. Imaging, ninety degree, p_0 = 0. This figure illustrates wavefront extrapolation in retarded non–slanted coordinates. In (a) the correct extrapolation velocity is used. All rays arrive at the imaging point in phase. In (b) the extrapolation velocity is 5 % slower. In (c) we are using a 5 % faster velocity. As we downward continue the wavefront, energy moves towards the zero offset region. Also note in this figure that velocity errors are emphasized at wide angles.

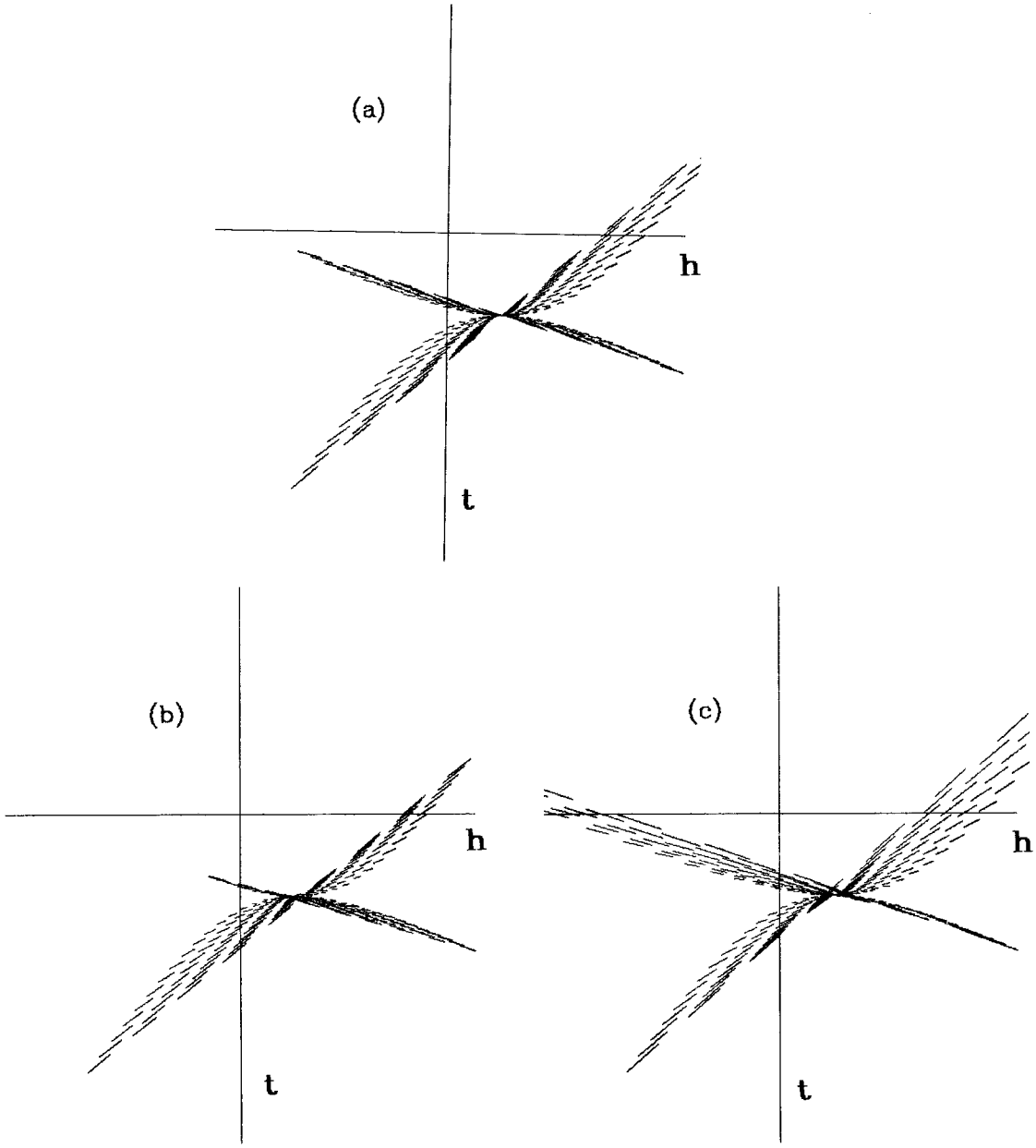

FIGURE 5.2. Imaging, ninety degree. $p_0 \neq 0$. This figure illustrates wavefront extrapolation in retarded Snell midpoint coordinates. The figure is for exact group velocity equations in Snell coordinates. At the surface we used an angle $\vartheta = 30^0$ for the linear moveout correction (equation 4.1a). In (a) the correct extrapolation velocity is used. All rays arrive at the imaging point in phase. In (b) the extrapolation velocity is 5 % slower. In (c) we are using a 5 % faster velocity. As we downward continue the wavefront, the energy moves toward the top of the skewed hyperboloid independent of the extrapolation velocity. Note that when the velocity is incorrect, high p values emphasize errors in the direction which energy moves.

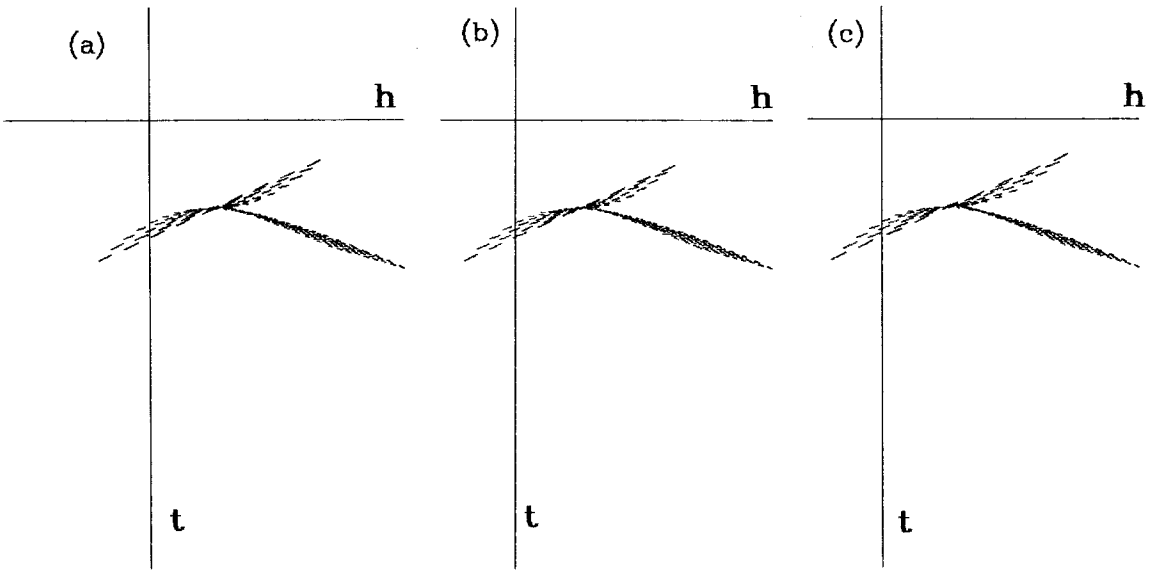

FIGURE 5.3. Imaging, fifteen degree. $p_0 \neq 0$. Imaging is done in Snell midpoint coordinates for a range of 60^0 about the reference wavefront slanted at 30^0. (a) has the right velocity, (b) a 5% underestimation and (c) 5% overestimation. There is little difference among the figures, so even though imaging is poor, the fifteen degree equation is particularly insensitive to errors in velocity in slanted coordinates.

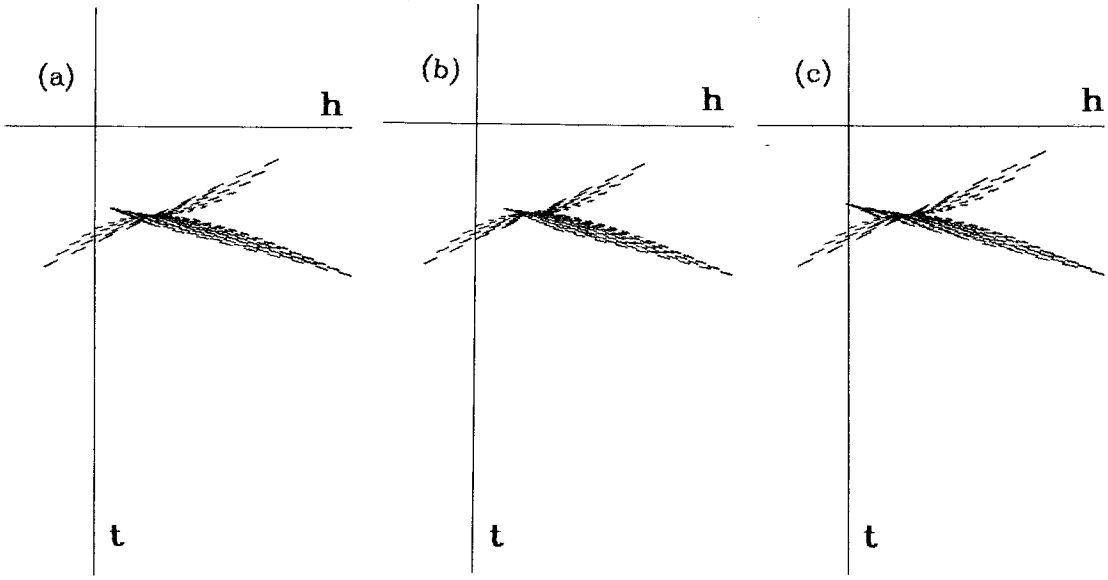

FIGURE 5.4. Imaging, forty–five degree. $p_0 \neq 0$. The imaging is done in Snell midpoint coordinates for a range of 60^0 about the reference wavefront slanted at 30^0. (a) has the right velocity, (b) 5% underestimation and (c) 5% overestimation. This approximation is more sensitive to errors in velocity. No apparent improvement in imaging is expected, compared to the fifteen degree equation, when imaging in slanted coordinates.

2.6. Conclusion

From the examples presented in this chapter, Snell midpoint coordinates prove to be a useful frame of reference when imaging events in *CMP* gathers. The linear moveout correction reduces high stepouts in the recorded data (in the positive range of offsets). Wavefield extrapolation operators are more sensitive to velocity at high stepouts, so this feature reduces errors. Downward continuation and imaging in Snell midpoint coordinates keeps the arrival coordinates of the reference Snell wavefront stationary. This is critical estimating velocity. Wave approximations are also fitted about a slant propagating wavefront. They can handle steeply traveling energy better than any non–slanted coordinate frame, and we do not need accurate operators oversensitive to velocity.

We have also learned that exact operators for wavefield extrapolation are useful only when we have exact velocity functions. There is always a trade off between accuracy of operators in imaging energy and accuracy in velocity functions. When there is a wide range of uncertainty in velocity, a low order approximation operator should suffice. Only as uncertainty in velocity decreases, does it pay to increase the accuracy, and therefore the cost, of the operators.

Finally, in slanted extrapolation the fifteen degree equation gives satisfactory results. The forty–five degree equation does not appreciably improve resolution.

Appendix A.

In this Appendix we derive dispersion relations for the exact acoustic wave equation and its two most commonly used one–way approximations. We apply equations derived in section (3) to find their associated group velocity relations.

The two–dimensional acoustic wave equation in half offset–time coordinates, in a constant velocity medium and in the absence of external sources, is given by

$$\left[\frac{\partial^2}{\partial h^2} + \frac{\partial^2}{\partial z^2} - \frac{1}{v^2} \frac{\partial^2}{\partial t^2} \right] f(h,z,t) = 0 \qquad \text{(A.1)}$$

where f represents the acoustic wavefield.

Introducing the Fourier Transform:

$$F(k_h,k_z,\omega) = \int_{-\infty}^{\infty}\int\int f(h,z,t)\, e^{-ik_h h - ik_z z + i\omega t}\, dh\, dz\, dt \qquad \text{(A.2)}$$

$$f(h,z,t) = \frac{1}{(2\pi)^{3/2}} \int_{-\infty}^{\infty}\int\int F(k_h,k_z,\omega)\, e^{ik_h h + ik_z z - i\omega t}\, dk_h\, dk_z\, d\omega \qquad \text{(A.3)}$$

we obtain

$$\left[k_h^2 + k_z^2 - \frac{\omega^2}{v^2} \right] F(k_h,k_z,\omega) = 0 \qquad \text{(A.4)}$$

Substituting for the definitions of p and q from equation (2.2) we get the *dispersion relation*

$$p^2 + q^2 - \frac{1}{v^2} = 0 \qquad \text{(A.5)}$$

To find approximations to this exact wave equation, we use *Muir's* expansion (Claerbout, 1982). This expansion is a recursion for the square root

$$R = (1 - X^2)^{1/2}$$

The initialization depends on angle, $R_0 = \cos\vartheta$, for zero degrees

$$R_0 = 1$$

$$R_{n+1} = 1 - \frac{X^2}{1 + R_n} \tag{A.6}$$

We can use equation (A.6) to find approximations of (A.5). The fifteen degree equation is given by the first term,

$$q \approx \frac{1}{v} - \frac{p^2 v}{2} \tag{A.7}$$

The next term gives the forty–five degree dispersion relation,

$$q \approx \frac{1}{v} \frac{1 - \frac{3}{4}p^2v^2}{1 - \frac{1}{4}p^2v^2} \tag{A.8}$$

Ninety degree equation. To find the group velocity equations, differentiate equation (A.5) with respect to p and q, giving

$$\frac{\partial F}{\partial p} = 2p$$

$$\frac{\partial F}{\partial q} = 2q$$

Therefore, from equation (2.5)

$$\lambda = (2p^2 + 2q^2)^{-1} = \frac{v^2}{2}$$

and applying equations (2.3) we get the ray equations

$$\frac{dh}{dt} = pv^2 \tag{A.9a}$$

$$\frac{dz}{dt} = qv^2 \tag{A.9b}$$

Fifteen degree equation. Differentiating equation (A.7) with respect to p and q we get

$$\frac{\partial F}{\partial p} = pv$$

$$\frac{\partial F}{\partial q} = 1$$

Solving for λ we get

$$\lambda = \left[p^2 v + q \right]^{-1} = \frac{2v}{p^2 v^2 + 2}$$

The ray equations are

$$\frac{dh}{dt} = \frac{2pv^2}{p^2 v^2 + 2} \tag{A.10a}$$

$$\frac{dz}{dt} = \frac{2v}{p^2 v^2 + 2} \tag{A.10b}$$

Forty-five degree equation. Differentiating equation (A.8) with respect to p and q we get

$$\frac{\partial F}{\partial p} = \frac{pv}{(1 - \frac{1}{4} p^2 v^2)^2}$$

$$\frac{\partial F}{\partial q} = 1$$

For λ we obtain

$$\lambda = \frac{v\,(1 - \frac{1}{4}p^2v^2)^2}{1 + \frac{3}{16}p^4v^4}$$

The ray equations become

$$\frac{dh}{dt} = \frac{pv^2}{1 + \frac{3}{16}p^4v^4} \qquad \text{(A.11a)}$$

$$\frac{dz}{dt} = \frac{v\,(1 - \frac{1}{4}p^2v^2)^2}{1 + \frac{3}{16}p^4v^4} \qquad \text{(A.11b)}$$